PCB PIEZOTRONICS
AN AMPHENOL COMPANY

Development of a Smart Building Monitoring System

Written By

Andrew T. Gothard, Tennessee Technological University
Steven R. Anton, Tennessee Technological University
R. Craig Henderson, Tennessee Technological University
Matthew Cardinal, PCB Piezotronics
Andy Taggart, PCB Piezotronics

Development of a Smart Building Monitoring System

1 Introduction

1.1 Overview of Smart Buildings and Structural Dynamics Monitoring Systems

Advances in sensor technology and computing power have revolutionized Structural Health Monitoring (SHM) and Structural Dynamics Monitoring (SDM), enabling real-time monitoring of urban areas, critical civil infrastructure sites, and prominent buildings for structural dynamics, structural health, and occupant safety performance [1]. SHM focuses on long-term monitoring to detect structural damage, while SDM tracks dynamic responses to factors like seismic activity and occupant movement. These technologies are increasingly applied to smart buildings to enhance structural integrity and occupant safety. At Tennessee Technological University's Ashraf Islam Engineering Building (AIEB), advanced SDM systems, embedded during construction for optimal placement, monitor localized human-induced vibrations and global structural behavior. Using a combination of accelerometers and strain gages, these systems capture detailed data from small-scale impacts, such as footsteps, to large-scale events, like seismic loads. Beyond safety, these systems also offer potential applications in occupant tracking, fall detection, and energy efficiency [9-13]. Additionally, the AIEB system addresses research gaps in areas such as wave propagation in complex media and combined strain-acceleration data for seismic monitoring, offering valuable insights for advancing building safety and human-building interaction research.

1.2 Ashraf Islam Engineering Building SDM Systems

Tennessee Technological University (TTU) is constructing a new facility for its Engineering Department, the Ashraf Islam Engineering Building (AIEB.) TTU took advantage of this construction by collaborating with the design and construction teams to incorporate multiple measurement systems directly into the structure of the new facility. This approach offers significant advantages over post-construction installations, as it allows for optimal mounting of the instrumentation for improved transducer responses.

The AIEB features two distinct SDM systems to allow for maximum short- and long-term versatility and offer multiple methods for SDM education and research. Upon completion, the AIEB will be the most heavily instrumented SDM system in the world, with 235 accelerometers and 88 strain gages between both the L-SDM and G-SDM systems. The two systems will be reviewed in the next sections.

1.2.1 AIEB Local-SDM System

The AIEB L-SDM systems is designed to monitor and study localized human-induced floor vibrations. The system utilizes uniaxial accelerometers mounted beneath the composite concrete floor. Sensor locations are shown in Figure 2. The L-SDM system is located in an adaptive learning room (ALR), which is carpeted, and in a hallway with a polished concrete floor. The ALR has 112 uniaxial accelerometers, while the hallway has 27. A mix of PCB J352B piezoelectric ICP sensors and Endevco 7201-50-R piezoelectric charge sensors are used. The sensors are mounted in two different ways; the first method involves mounting to the bottom face of the structural beams using a mounting block, while the second involves mounting to the profile steel

deck (PSD) using mounting blocks and concrete screws. The sensor locations, types, and mounting methods were chosen to allow for maximum future flexibility in testing methods. Overall, the L-SDM system is well-suited for studying wave propagation in complex media, occupancy monitoring and fall detection/safety monitoring.

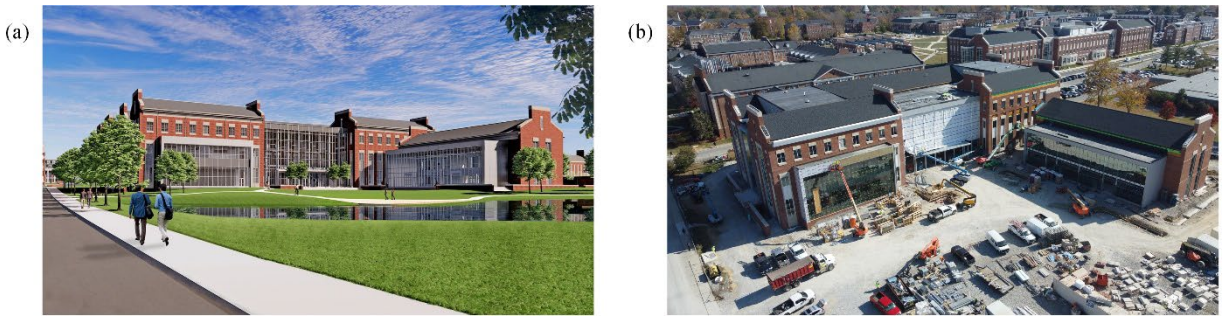

Figure 1: The Ashraf Islam Engineering Building (AIEB) at Tennessee Technological University (TTU) showing (a) an architectural rendering and (b) an image taken during construction (on November 6th, 2023).

1.2.2 AIEB Global-SDM System

The AIEB G-SDM system measures the building's structural behavior when subjected to seismic and vibratory loads by gathering strain and acceleration data at key points in the lateral force resisting system (LFRS). The LFRS in the AIEB consists of moment frames, which are beams and columns constructed with connections that resist flexure. The G-SDM system includes 44 sensors spread throughout the LFRS (Figure 3a). Sensors are mounted at the beam-to-column connection points. In order to measure the worst-case stresses on columns and beams, two Geokon 4000 vibrating wire strain gages are placed symmetrically on the flanges of the LFRS members at all 44 locations. Additionally, a single Endevco 773-2-R variable capacitance (VC) MEMS triaxial accelerometer is mounted on the web of the beam or column member at sensor locations on the second and third floors of the AIEB. A diagram showing the accelerometer and strain gage placement on a column can be seen in Figure 3. It should be noted that no triaxial accelerometers are installed on the first-floor column bases because far-field accelerometers will be used to collect data regarding ground acceleration. Two far-field accelerometers will be placed outside of the building, and one will be placed in the basement to gain insight into how seismic ground motion propagates through the surrounding soil medium and disperses through the structure.

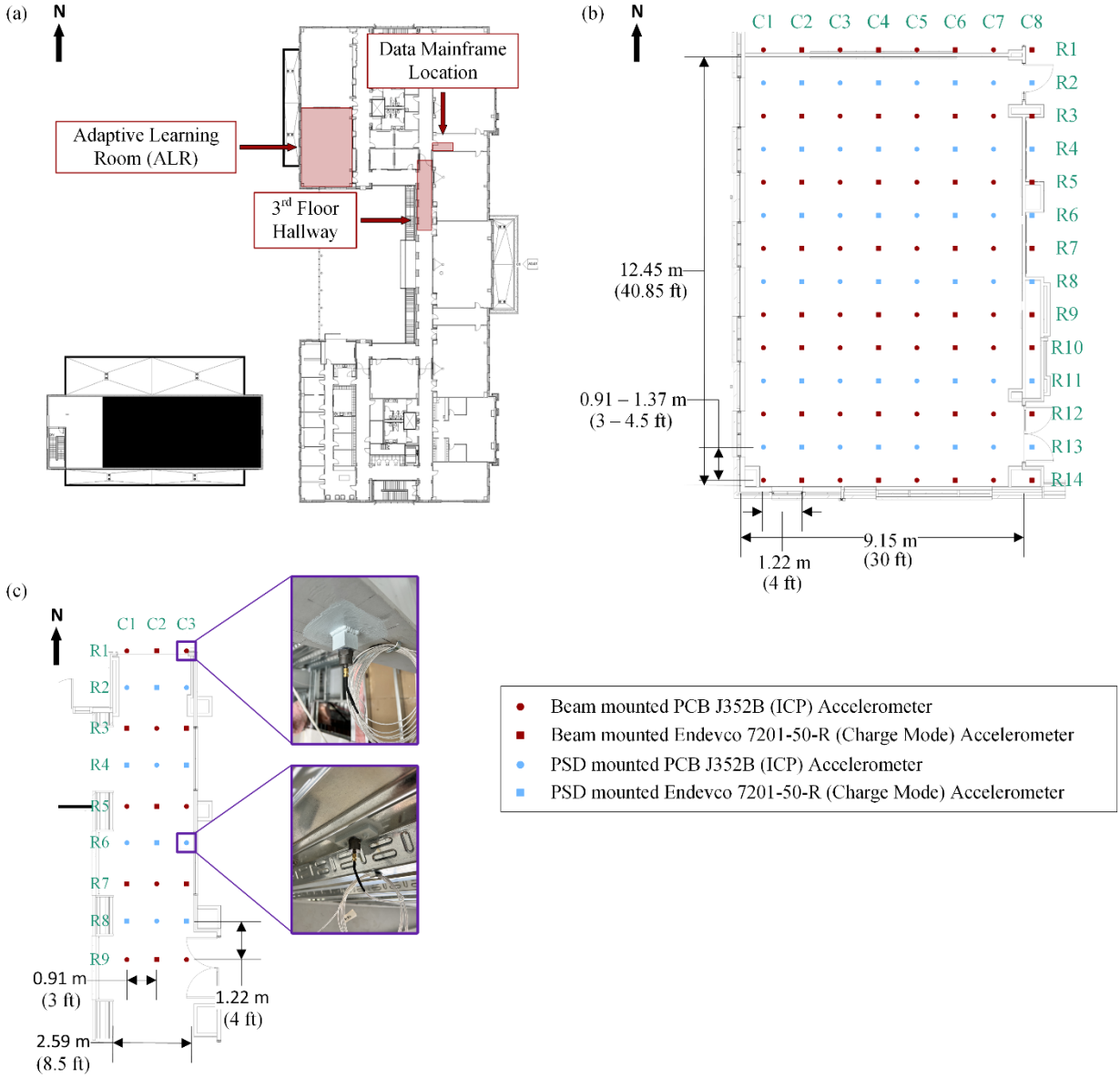

Figure 2: AIEB L-SDM system showing (a) the location of the L-SDM system on the third floor of the north wing of the AIEB, (b) the accelerometer layout in the Adaptive Learning Room (ALR), and (c) the accelerometer layout in the hallway.

2 Methods

2.1 Sensor Selection

The AIEB L-SDM system will be used to detect and monitor human-induced accelerations propagating through the floor of the building. In order to accurately capture these vibrations, there are several design requirements. When selecting the appropriate accelerometers, the primary concern was to allow for flexibility to measure multiple types of events. The systems would need to be able to measure relatively low-energy events from human induced vibrations, such as walking and running. The sensors also needed to be able to measure relatively high-energy events, such as impacts from dropped objects and falls. Testing

was completed to attempt to determine a range for both low-energy and high-energy events. Testing showed that low-energy events had amplitude ranges of 2.48-7.59 mg. Sensors mounted on PSD locations had frequency components from 0-12.8 kHz, while the beam-mounted locations had frequency components from 0-1 kHz. High-energy events had amplitude ranges from 5g-25g. In addition to maximizing flexibility, the sensor selection criteria also included requirements to be resistant to electrical noise from facility components, and to have a life expectancy of over 30 years to provide reliable performance for long-term research.

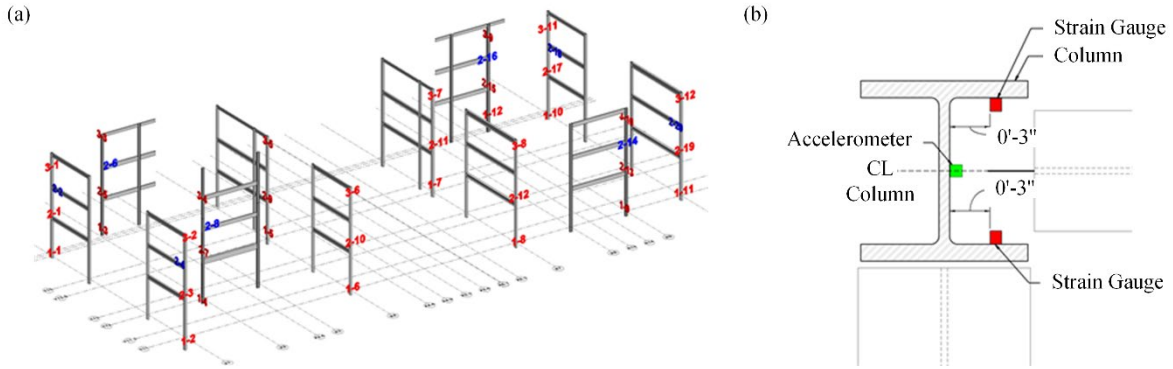

Figure 3: AIEB G-SDM system showing (a) 44 sensor locations on the LFRS and (b) diagram of accelerometer and strain gage layout for the sensor locations (note, first floor locations do not have accelerometers).

Table 1: AIEB L-SDM System Sensor Specifications

Sensor	Type	Sensitivity	Measurement Range	Frequency Range	Shock Limit
PCB J352B	Uniaxial accelerometer, ICP	1000 mV/g	$\pm$ 5 $g\ pk$	1-15000 Hz	$\pm$ 1000 g pk
Endevco 7201-50-R	Uniaxial accelerometer, charge mode	50 pC/g	$\pm$2000 $g\ pk$	1-6000 Hz	$\pm$ 10000 g pk

Based on the results from the preliminary study and the selection criteria, two types of accelerometers were selected for the AIEB L-SDM system: the PCB J352B ICP accelerometer and the Endevco 7201-50-R charge mode accelerometer. The specifications of both accelerometers can be seen in Table 1. A combination of accelerometers was selected to make the system more versatile and able to measure both low and high-energy events from human-building interactions without needing to change the sensors or modify the instrumentation after installation and construction were completed. The PCB J352B ICP accelerometer was chosen because it has a high sensitivity and a broad frequency range, meaning that it can measure the low amplitudes and high frequency content seen in the preliminary testing. Additionally, ICP accelerometers are inherently resistant to electrical interference, as they convert the standard piezoelectric high impedance output to a low impedance output. ICP sensors require relatively inexpensive power supplies compared to charge mode piezoelectric sensors.

These characteristics make the PCB J352B an ideal accelerometer to measure the low amplitude vibrations caused by footsteps, which are expected to be the lowest energy events of interest that will be measured by the L-SDM system. The PCB J352B accelerometers also have a high shock limit of ±1000 g pk, which means they will not be damaged by short-term, high-energy events experienced in the building.

While the PCB J352B accelerometers are excellent for measuring low amplitude accelerations, they are not sufficient for measuring high-energy events in the L-SDM system since their measurement range only

extends up to ±5 g pk and the preliminary impact testing showed accelerations up to 25 g. A charge mode accelerometer, the Endevco 7201-50-R, was chosen for use in the system to measure a wider range of acceleration amplitudes for high-energy events. During the design and planning process for the measurement system, the expected acceleration values were preliminary and predicted. Actual measurement data from the specific mounting locations and test site were not available as the project was under construction, and sensors would need to be mounted during the construction phase. In order to maximize the flexibility of the systems and ensure the measurement range of the sensors could be tailored to the final measured values of the installed system, piezoelectric charge mode sensors were also selected to be incorporated into the measurement system. The Endevco 7201-50-R has an overall measurement range of ±2000 g pk and a high (and adjustable) sensitivity. By changing the gain of the sensor with a charge amplifier or charge convertor, the user can adjust the system sensitivity and range. This allows for additional customization during testing, and ensures the measurement range of the sensors can be set based on actual measurement data. This type of accelerometer also has a high shock limit and will not be damaged by the high-energy events experienced by the L-SDM system. Overall, the combination of the PCB J352B and Endevco 7201-50-R accelerometers provides a broad range of measurement capabilities and flexibility suitable for the wide range of research studies envisioned with the AIEB L-SDM system.

2.2 Cable Selection

The primary criteria for the sensor cables was the ability to effectively transport the sensor signals over long cable runs up to 150 ft. in length. An additional requirement was to be durable enough to be installed in a construction environment, and allow for field installable connectors. PCB Model 032 coaxial cable with a single twisted pair of 30 AWG stranded wire and a braided shield was selected for the AIEB L-SDM system. The PCB 032 cable's twisted pair wiring configuration makes the cable resistant to electrical noise. The stranded wire cable also makes the wire flexible and fatigue-resistant, which is crucial during the installation process, where wires are frequently moved and re-routed. The resistance per foot and capacitance per foot of the PCB 032 cable is also appropriate for both ICP and charge mode accelerometers in an environment where the sensors are permanently installed with cable runs up to 150 ft. and frequency ranges up to approximately 10,000 Hz with 3 mA of power supplied to the sensors. Longer cable runs are technically feasible, but exact lengths are dependent on the required frequency range of the measurement along with the current available for powering the sensor. It should be noted that a second type of cable is used in the AIEB L-SDM system to connect the output of signal conditioners placed within the ALR to the input of the data acquisition mainframes placed in the data mainframe location (details of cable routing omitted here for brevity). In short, the northernmost seven rows of sensors in the ALR (rows 1-7) will have their signal conditioners placed within the ALR, while the southernmost seven rows (rows 8-14) will have their signal conditioners placed within the data mainframe location (along with all hallway sensors.) This allows studies into the effect of cable length on sensing system performance. As such, a more cost-effective solution cable, L-COM TSFC6, a Category 6 cable with four twisted pairs of 26 AWG stranded wire, an inner foil shield, and an exterior braided shield, was chosen.

2.3 Experimental Validation of AIEB

At the time of this paper being written, all 139 accelerometers (shown in Figure 2) have been mounted for the L-SDM system, and all cable has been run. An initial walking analysis and impact test have been completed, and results are discussed below.

2.3.1 Walking Analysis

The walking analysis was conducted in both the ALR and hallway through multiple walking trials. A 68 kg (156 lb) male, wearing soft-soled shoes, walked from South to North in columns across both areas. The resulting accelerations were recorded for post-processing. The full system was not completed yet for all

areas, and it is expected that the stiffness of the floor in the ALR will vary. Two groups of accelerometers were tested to ensure representative performance. In each accelerometer group, there are four accelerometers, which represent each combination of accelerometer type (i.e., PCB J352B, Endevco 7201-50-R) and mounting location (i.e., beam-mounted and PSD-mounted) in the AIEB L-SDM system. Diagrams showing approximate accelerometer and walking column locations for the ALR and hallway can be seen in Figure 4(a) and (b), respectively. The stiffness of the hallway is expected to be relatively uniform across the instrumented section since the hallway is much narrower than the ALR. Only one group of accelerometers is selected for the hallway, which is labeled as hallway group 1 (H-G1) and consists of H6-1, H6-2, H7-1, and H7-2 accelerometers. These accelerometers are chosen because they are located near the mid-section of the hallway, allowing for space to perform walking trials that span across each side of the accelerometer.

It should be noted that the Endevco 7201-50-R accelerometers were not considered in the walking trial analysis, because they are included in the AIEB L-SDM system mainly to observe high-energy impacts such as falls. For the walking trials, accelerations from each group of accelerometers were recorded using the experimental setup shown in Figure 4(c). The ICP accelerometer signals were conditioned using a PCB 483C41 signal conditioner with AC coupling, configured as an ICP power supply with 4 mA of constant current excitation. The output voltages from the signal conditioner were then acquired using a National Instruments (NI) 9234 DAQ card placed within a compact DAQ (cDAQ-9171) chassis, and a laptop running a custom LabVIEW code. The sampling rate was set to 51.2 kHz, the maximum sampling rate for the NI 9234 DAQ card, to capture frequencies up to 25.6 kHz during the frequency analysis. Since long cables (>100 ft.) were used in the AIEB L-SDM system, high-frequency attenuation could occur due to the capacitive filtering effect of the cables. Thus, it was essential to estimate the theoretical upper frequency limit of the system and ensure appropriate signal conditioning. The theoretical upper frequency limit was estimated based on the maximum ICP accelerometer cable length in the AIEB L-SDM system (approximately 140 ft.) and the level of constant current excitation provided to the sensors (4 mA), and found to be approximately 35 kHz—well above the 25.6 kHz resolvable frequency range of the DAQ setup (details of the formula for computing the upper frequency limit can be found in Ref [16]). For each walking column, 10 walking trials are performed in the evening to avoid construction noise and establish averages and confidence bounds.

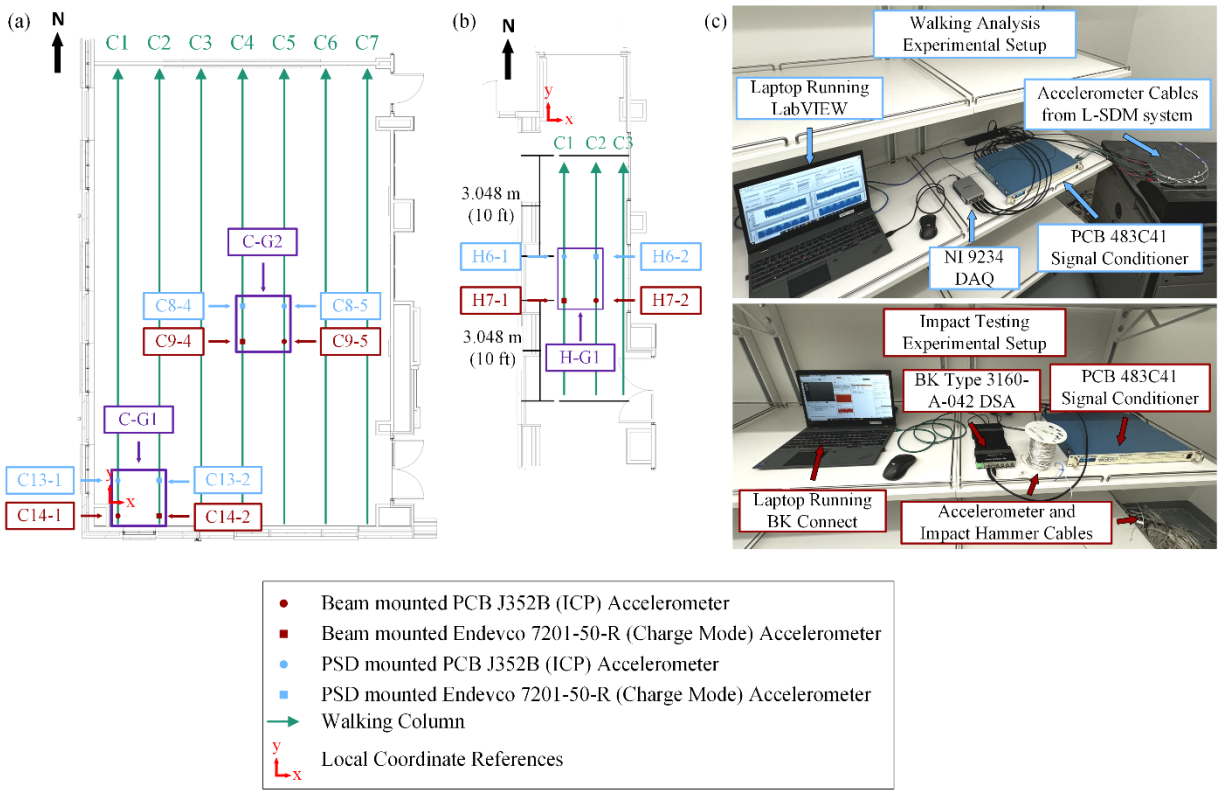

Figure 4: AIEB walking analysis and impact testing setup showing approximate sensor locations and walking columns in (a) ALR and (b) hallway, and (c) data acquisition setup.

2.3.2 Impact Testing

Impact testing was used to study the response of the AIEB L-SDM system to high-energy events and validate the selection of accelerometers within the system. It is important to note that the PCB J352B accelerometers are excluded from this analysis because the acceleration measurements from hammer impacts are found to be above the measurement range of the accelerometers (i.e., ± 5 g). The impact testing experimental setup was similar to the walking analysis, as shown in Figure 4(c). Instrumented hammer impacts on the floor were used to simulate high-energy events. The impact analysis was conducted using the same groups of accelerometers for the ALR and hallway as in Section 2.3.1. The tests were performed by impacting the floor at the driving point of each accelerometer using a PCB model 086D20 impact hammer with a black tip. The charge mode accelerometer signals were conditioned using a PCB 483C41 signal conditioner with AC coupling, configured as a charge amplifier with the gain set to 1 mV/pC. In order to understand the general response of the system to the high-energy impact loading, frequency response functions (FRFs) were calculated for each location assuming a linear, time-invariant system. A Brüel & Kjær (B&K) Type 3160-A-042 digital signal analyzer (DSA) running BK Connect software was used to collect and process the FRF data. The sampling rate, block size, frequency span, and frequency resolution were set to 3.2 kHz, 3.2 s, 0-1 kHz, and 0.3125 Hz, respectively. The frequency range was selected based on the fact the black impact hammer tip is generally able to excite frequencies between 0-1 kHz. Then, an appropriate sampling rate was chosen from a set of pre-defined rates in BK Connect to avoid aliasing. The block size was selected so that the hammer and accelerometer signals naturally decay out within the specified block size. This fulfills the periodicity requirement of the FRF calculation so windows do not need to be applied to the data. Linear averaging was used to calculate each FRF, and 10 averages were used for each location. A 10 kN trigger was also applied so that sufficient force was used to excite the desired frequency range. Finally, maximum

force and acceleration ranges were calculated from the hammer impact time-domain data in order to verify the selection of accelerometers in the AIEB L-SDM system.

3 Results

3.1 Walking Analysis

The walking trials were first evaluated visually to determine whether footsteps were identifiable in the time-domain. Representative walking trial time-domain graphs for C13-1, C14-1, C8-5, C9-5, H6-1, and H7-2 sensors are shown in Figure 5. The representative graphs are from trials where the walking column directly crossed over each sensor. Graphs from other columns displayed similar trends, except with lower amplitudes as the walking columns moved away from the accelerometer location. Based on the time-domain data, footsteps were visible for all sensors except for C14-1.

A time-frequency analysis was then performed on each walking trial to observe the frequency content associated with the footsteps during testing. Spectrograms were computed up to 25.6 kHz, which is the maximum measurable frequency for a sampling rate of 51.2 kHz. It should be noted that the PCB J352B's specifications only recommend using the sensors across a maximum frequency range of 1-15,000 Hz (error ±10%); however, since this analysis focused only the presence of higher-frequency content and not the accuracy of amplitude, the full frequency range of the spectrograms was considered. The spectrograms were calculated using MATLAB's 'pspectrum' command with the following parameters: a time resolution of 0.05 s (approximately half of the observable signal duration for footsteps), a 20% overlap, and a Kaiser-Bessel window with a constant of 0.7. Representative spectrograms for the C13-1, C14-1, C8-5, C9-5, H6-1, and H7-2 sensors are shown in Figure 5. Looking at the spectrogram results for each sensor location, most of the frequency content in all spectrograms was below 1 kHz. However, for all accelerometers except C14-1, footsteps were visible up to 25.6 kHz, with high-frequency amplitudes often being low but still present. The overall frequency range calculated for footsteps in the AIEB was then 0-25.6 kHz.

Next, the walking analysis trials were evaluated to determine the average maximum acceleration for each walking column for each accelerometer. An overall average range of maximum acceleration values for footsteps for each accelerometer group was also calculated. The maximum acceleration for each walking trial was determined by taking the absolute value of the entire signal and finding the maximum acceleration value. The maximum accelerations for each trial were then averaged for each accelerometer on a column-by-column basis, and 90% confidence intervals were determined. The resulting average maximum acceleration values for each column in the ALR and hallway are shown in Figure 6. Note that trial 4 from column 1 of the hallway trials was removed due to an acceleration spike that was determined to be an outlier. Moving forward with the analysis, the range of average maximum acceleration for the ALR and hallway accelerometer groups was taken as the range between the lowest and highest average maximum acceleration values in each group. The range of average maximum accelerations for C-G1, C-G2, and H-G1 were 1.2-2.1 mg, 1.5-2.8 mg, and 2.3-3.7 mg, respectively. An overall maximum average acceleration range from the experimental walking trials for the L-SDM system was therefore approximately1.2-3.7 mg, which provides an estimate of the maximum accelerations expected for low-energy footstep events in the AIEB L-SDM system.

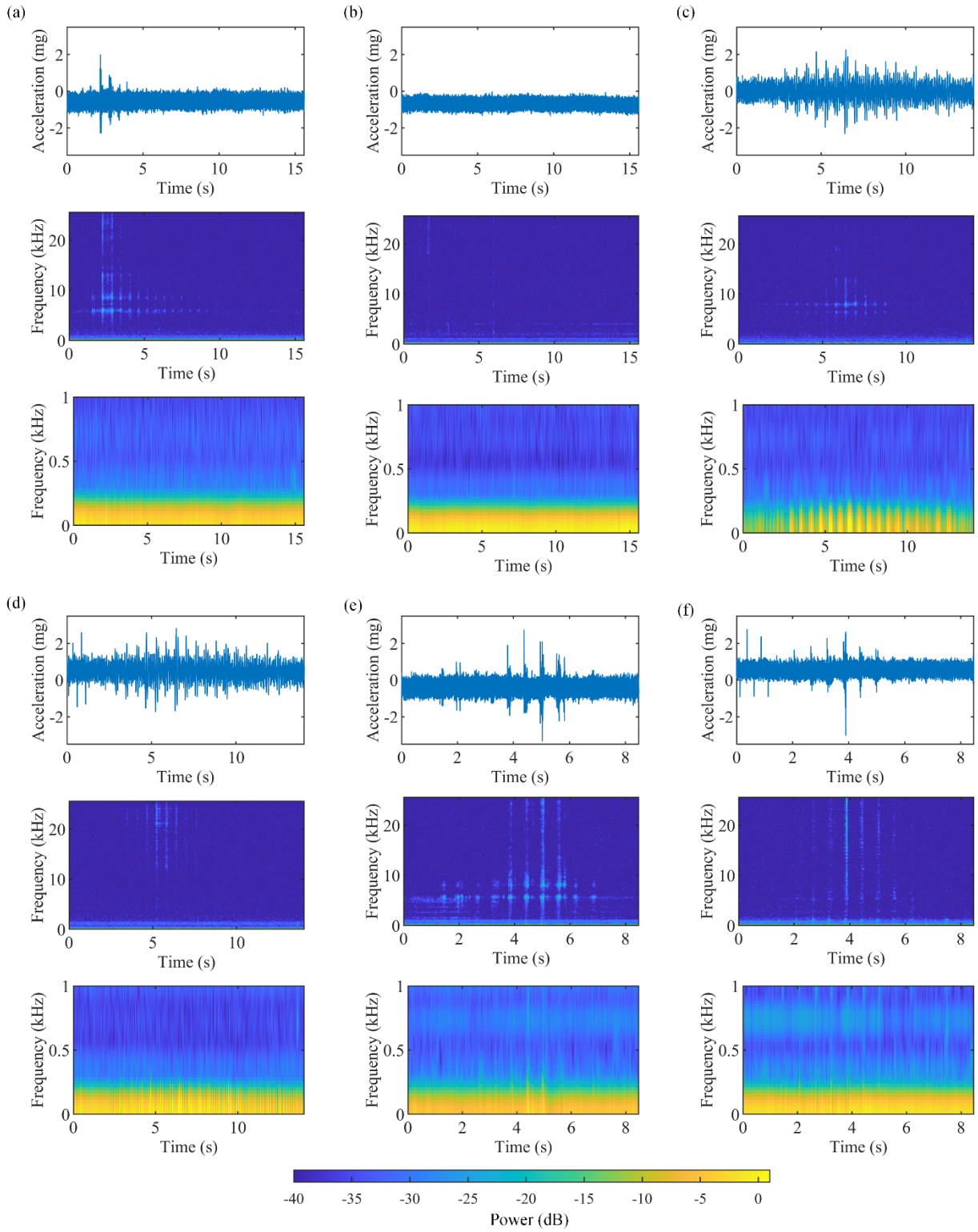

Figure 5: Representative ALR and hallway walking trial time responses and corresponding spectrograms for (a) C13-1 column 1 trial 1, (b) C14-1 column 1 trial 1, (c) C8-5 column 5 trial 1, (d) C9-5 column 5 trial 1, (e) H6-1 column 1 trial, and (d) H7-2 column 2 trial 1.

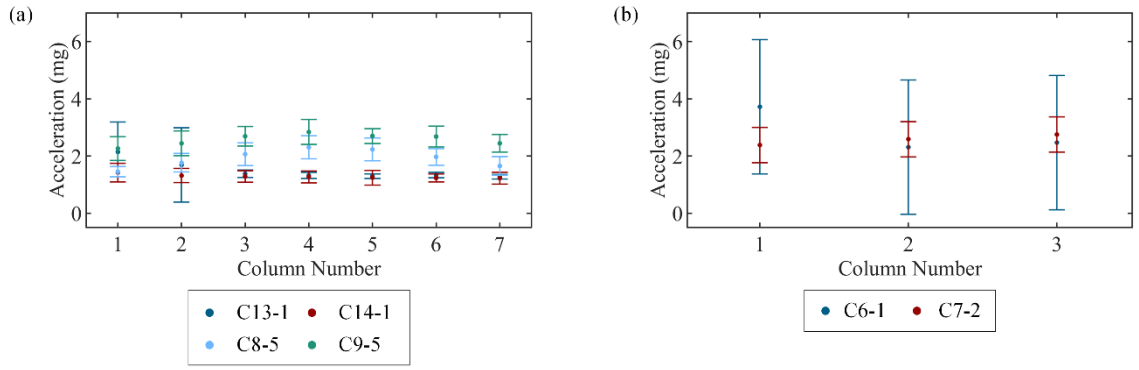

Figure 6: Average maximum accelerations per column with 90% confidence intervals for (a) the ALR and (b) the hallway.

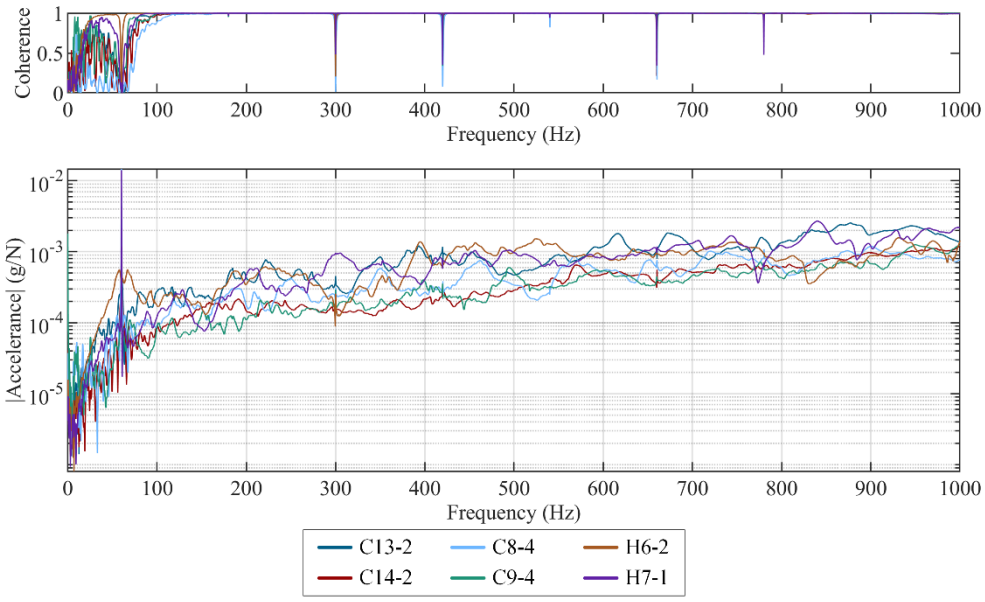

Figure 7: Impact testing results for all impact locations showing (a) coherence and (b) accelerance frequency response functions (FRFs).

3.2 Impact Testing

The FRF results from the impact testing for each charge mode accelerometer location are shown in Figure 7. Based on these results, several observations can be made. First, all FRF plots show a general increase in response with an increase in frequency, which is typical for vibration in dynamic systems [17].

In addition to the FRFs, maximum force and acceleration ranges were also calculated from the hammer impact data in the time-domain. This analysis helped verify the selection of accelerometers in the AIEB L-SDM system and to compare the results to the preliminary analysis performed by Hott [15]. The maximum force and acceleration ranges from all 60 impact tests were determined to be 10-19.5 kN and 3-14.4 g, respectively.

4 Discussion

4.1 Walking Analysis

Several notable observations were made from the walking analysis results. First, the time-domain data of the representative walking trials in Figure 5 shows that footsteps are distinguishable for each sensor except C14-1, suggesting that the stiff corners of the classroom may be suboptimal for footstep detectability. This will be investigated in future studies. Next, the time-frequency graphs in Figure 5 reveal that the majority of the frequency content from footstep excitation is below 1 kHz. This is consistent with the preliminary analysis done by Hott, as well as other previous literature [15, 18]. In this frequency range, footsteps were visually identifiable for each accelerometer except for C13-1 and C14-1, likely due to the fact that the accelerometers are located in the corner of the room where the response is expected to be the lowest. The center accelerometers in the ALR, C8-5 and C9-5, have peaks that are particularly clear in the lower frequency band, more so than in the hallway, which can be seen in Figure 5(c) and (d). The authors believe that this may be caused by the lower stiffness in the center of the floor; considering the FRF plot of a simple second-order model as an example, a lower stiffness would shift the resonance to a lower frequency and allow larger response at low frequencies. Next, for the high frequency content above 1 kHz, the spectrograms of all accelerometers except C14-1 showed visible evidence of footsteps up to 25.6 kHz. The high frequency amplitudes are often low, but still present. The hallway accelerometers, H6-1 and H7-2, have peaks that were particularly clear in the high frequency band, more so than in the classroom. Finally, PSD-mounted locations showed more distinguishable footstep content in both time and frequency domains than beam-mounted locations across all three areas tested. In fact, two frequency bands are present for PSD-mounted sensors that clearly display footstep data, one around 6 kHz and another around 8 kHz. These frequency bands may provide an advantage for footstep detectability, and will be investigated in future studies.

Next, the average maximum acceleration results for each column in Figure 6 showed that the average maximum acceleration for C-G2 accelerometers was generally higher than C-G1 accelerometers, even for columns closer to the C-G1 sensors. This is likely due to the increased stiffness in the corner of the room, indicating that accelerometers located in more compliant areas (e.g., the room's center) provide better sensing capabilities for footsteps. Looking at the results from the hallway, the average maximum acceleration range for H-G1 (2.3-3.7 mg) is higher than that of C-G2 (1.5-2.8 mg). Additionally, the confidence bounds for the average maximum acceleration are larger in the hallway than in both classroom locations, indicating a larger range of expected accelerations. The higher average maximum acceleration range and larger variability in the hallway may be due to differences in flooring types. The surface of the hallway is polished concrete, while the classroom is carpeted. Carpet damping affects the overall acceleration amplitudes, reducing the upper limit of acceleration amplitudes, and, ultimately, reducing the spread of average maximum acceleration. Comparing PSD and beam-mounted locations, there are no significant differences in average maximum acceleration. However, differences became apparent in the impact testing results, which will be discussed in the next section.

4.2 Impact Testing

Similar trends were observed in the impact testing results as in the walking analysis. First, as shown in Figure 7, the largest responses occurred at the PSD-mounted accelerometers in the corner of the classroom and hallway locations, while the lowest responses are seen from the beam-mounted locations in the classroom. Interestingly, the hallway locations showed similar responses for both beam and PSD-mounted accelerometers, whereas in the classroom, the PSD-mounted locations had higher responses than either of the beam-mounted locations. Overall, the differences in responses show that each mounting type and location may have advantages in particular applications related to human-building interactions. This supports the decision to use multiple instrumented locations and mounting types within AIEB L-SDM system, enabling the system to serve as a versatile research platform for various dynamic characterization

and accelerometer placement optimization studies. Future modal analysis studies will be used to better characterize, compare, and model the overall dynamic properties of the hallway and classroom, with particular focus on analyzing the low-frequency response of the system.

Next, the maximum force and acceleration ranges calculated from the time-domain hammer impact data were higher than those used in preliminary testing performed by Hott [15], sufficiently representing high-energy events in the L-SDM system. The maximum acceleration range in this study (3-14.4 g) is actually lower than the accelerations seen in Hott's preliminary analysis[15]. This is not unexpected, since the structure of the AIEB is different than the surrogate building used during the preliminary analysis. While the acceleration ranges are different, both are on the same order of magnitude. This validates the incorporation of Endevco 7201-50-R accelerometers into the AIEB L-SDM system, as the observed accelerations were outside of the measurement range of the PCB J352B accelerometer, but are several orders of magnitude below the upper limit of the Endevco 7201-50-R accelerometers (i.e. ±2000 g pk). Overall, the Endevco 7201-50-R accelerometers are well-suited to measure the high-energy events that will be observed in the AIEB L-SDM system.

5 Conclusions

The AIEB SDM system demonstrates the effectiveness of integrated structural monitoring technologies in a smart building environment. Initial tests, including walking and impact analyses, successfully identified key frequency ranges for footsteps (up to 25.6 kHz) and validated the sensor choices for both low-energy and high-energy events. The combination of PCB J352B accelerometers for low-energy events and Endevco 7201-50-R accelerometers for high-energy impacts provides the system with the flexibility to monitor a wide range of human-building interactions and dynamic loads. This comprehensive approach ensures the system can capture everything from subtle vibrations caused by footsteps to intense seismic forces. Moving forward, the system offers significant potential for future research, including optimizing sensor placement, refining wave propagation models, and expanding applications in occupant tracking, fall detection, and overall building safety. These initial results validate the AIEB SDM system as a versatile platform for improving both structural integrity and occupant safety, with broader implications for smart building technologies.

6 Acknowledgments

The authors would like to acknowledge Brad Nokes and Curtis Elkins from Denark Construction for their assistance with coordinating experimentation within the active construction site of the Ashraf Islam Engineering Building.

7 References

[1] Buckman, A. H., Mayfield, M., and Beck, S. B. M., (2014). "What is a Smart Building?" *Smart and Sustainable Built Environment*, 3(2), pp. 92-109.
[2] Verma, A., Prakash, S., Srivastava, V., Kumar, A., and Mukhopadhyay, S. C., (2019). "Sensing, Controlling, and IoT Infrastructure in Smart Buildings: A Review," *IEEE Sensors Journal*, 19(20), pp. 9036-9046.
[3] Lightner, M. R., Carlson, L., Sullivan, J. F., Brandemuehl, M. J., and Reitsma, R., (2000). "A Living Laboratory," *Proceedings of the IEEE*, 88(1), pp. 31-40.
[4] Snieder, R., and Safak, E., (2006). "Extracting the Building Response using Seismic Interferometry: Theory and Application to the Millikan Library in Pasadena, California," *Bulletin of the Seismological Society of America*, 96(2), pp. 586-598.
[5] Skolnik, D., Lei, Y., Yu, E., and Wallace, J. W., (2006). "Identification, Model Updating, and Response

Prediction of an Instrumented 15-Story Steel-Frame Building," *Earthquake Spectra*, 22(3), pp. 781-802.
[6] Çelebi, M., Toksöz, N., and Büyüköztürk, O., (2014). "Rocking Behavior of an Instrumented Unique Building on the MIT Campus Identified from Ambient Shaking Data," *Earthquake Spectra*, 30(2), pp. 705-720.
[7] Sarlo, R., Tarazaga, P. A., and Kasarda, M. E., (2018). "High Resolution Operational Modal Analysis on a Five-Story Smart Building Under Wind and Human Induced Excitation," *Engineering Structures*, 176, pp. 279-292.
[8] Skolnik, D. A., Ciudad-Real, M., and Swanson, D., (2017). "Engineering on Display at the New Engineering Industrial Building, University of Alaska - Anchorage," *Proceedings of the 16th World Conference on Earthquake Engineering*, pp. 4211.
[9] Poston, J. D., Schloemann, J., and Buehrer, R. M., (2015). "Towards Indoor Localization of Pedestrians via Smart Building Vibration Sensing," *Proceedings of the 2015 International Conference on Localization and GNSS (ICL-GNSS)*, pp. 1-6.
[10] Poston, J. D., Buehrer, R. M., and Tarazaga, P. A., (2017). "Indoor Footstep Localization from Structural Dynamics Instrumentation," *Mechanical Systems and Signal Processing*, 88, pp. 224-239.
[11] Poston, J. D., Buehrer, R. M., and Tarazaga, P. A., (2017). "A Framework for Occupancy Tracking in a Building via Structural Dynamics Sensing of Footstep Vibrations," *Frontiers in Built Environment*, 3, pp. 65.
[12] Wu, K., Huang, Y., Qiu, M., Peng, Z., and Wang, L., (2023). "Toward Device-Free and User-Independent Fall Detection Using Floor Vibration," *ACM Transactions on Sensor Networks,* 19(1), pp. 1-20.
[13] Bertero, S., Tarazaga, P. A., and Sarlo, R., (2022). "In Situ Seismic Testing for Experimental Modal Analysis of Civil Structures," *Engineering Structures*, 270, 114773.
[14] Fisher, S. G., (2024). *Experimental and Analytical Evaluation and Installation of Spatially Distributed Smart Building Sensors* [Master's thesis, Tennessee Technological University].
[15] Hott, J. W., (2024). *The Design and Implementation of an Underfloor Accelerometer-Based Local Structural Dynamics Monitoring System for the Ashraf Islam Engineering Building* [Master's thesis, Tennessee Technological University].
[16] PCB Piezotronics. "Driving Long Cables." https://www.pcb.com/resources/technical-information/driving-long-cables (accessed 2024).
[17] Avitabile, P. (2017). *Modal Testing: A Practitioner's Guide*. John Wiley & Sons.
[18] Ekimov, A., and Sabatier, J. M., (2006). "Vibration and Sound Signatures of Human Footsteps in Buildings," *The Journal of the Acoustical Society of America*, 120(2), pp. 762-76.

PCB PIEZOTRONICS
AN AMPHENOL COMPANY

3425 Walden Avenue, Depew, NY 14043 USA

pcb.com | info@pcb.com | 800 828 8840 | +1 716 684 0001

WPL_100_0725